ChemComm

COMMUNICATION

View Article Online
View Journal

Cite this: DOI: 10.1039/d6cc03254k

Received 27th May 2026,
Accepted 16th June 2026

DOI: 10.1039/d6cc03254k

rsc.li/chemcomm

Molecular design strategy for solution-phase magneto-chiral photochemistry

Kosuke Itaya,[a] Kaoru Koizumi,[a] Kota Inage,[a] Mengfei Wang,[bc] Kazuyuki Ishii,[d] Yasuchika Hasegawa,[bc] Shojiro Kimura *[e] and Yuichi Kitagawa *[bc]

We report the magneto-chiral dichroism (MChD) of chiral tetrakis-type Eu(III) complexes in organic media. The obtained magneto-chiral anisotropy factor ($|g_{MChD}| = 0.015\ T^{-1}$) is the highest reported to date for solution-phase systems, offering important insights into the future development of magneto-chiral photochemical applications.

The interplay between chirality and magnetism has been an area of intense research over the last few decades.[1–4] Among the reported chiral-magnetic optical phenomena, magneto-chiral dichroism (MChD)—the differential absorption or emission of unpolarized light by chiral systems when a magnetic field is applied parallel to the light wavevector—is particularly compelling.[1,5,6] The magneto-chiral anisotropy factor, g_{MChD}, is typically defined as

$$g_{MChD} = 2 \cdot \frac{I_{B\uparrow\uparrow k} - I_{B\uparrow\downarrow k}}{I_{B\uparrow\uparrow k} + I_{B\uparrow\downarrow k}} \cdot \frac{1}{B}$$

where I is the transition intensity (representing absorption or emission), subscript $I_{B\uparrow\uparrow k}$ denotes the intensity measured when the magnetic field (B) is parallel to the light wavevector (k), and subscript $I_{B\uparrow\downarrow k}$ denotes the intensity when B is antiparallel to k. Chiral compounds with large g_{MChD} values have unprecedented potential for use in magneto-optical devices and as novel physical sources for asymmetric photochemical reactions without chiral reagents.

Historically, Rikken and Raupach were the first to experimentally demonstrate MChD signals in luminescent and absorption transitions using chiral Eu(III) complexes[7] and nickel(II) sulfate,[8] respectively. The same author also demonstrated an MChD-based enantioselective photochemical reaction under a high magnetic field using Cr(III) complexes.[9,10] Following these findings, several researchers attempted to design chiral compounds with strong MChD effects using ceramics,[11–13] metal complexes,[14–27] and organic molecules.[28] For example, Atzori reported a chiral Prussian blue analog with a ferrimagnetic ordered state that has a high g_{MChD} value ($|g_{MChD}| = 0.026\ T^{-1}$, 4.0 K).[12] Dhbaibi detected a strong MChD signal ($|g_{MChD}| = 0.19\ T^{-1}$, 4.0 K) from Yb(III) coordination polymers incorporating helicene-based ligands with magnetic anisotropy.[21] Atzori and coworkers demonstrated an intense MChD signal ($|g_{MChD}| = 0.24\ T^{-1}$, 4.0 K) in the near-infrared region for the $^4I_{13/2} \rightarrow {}^4I_{15/2}$ transition in an Er(III) complex, owing to its magnetic anisotropy and large transition magnetic dipole moments.[23] However, large g_{MChD} values are generally limited to solid-state systems at cryogenic temperatures, where long-range magnetic ordering or pronounced single-ion magnetic anisotropy is present. The difficulty of realizing strong MChD effects in solution at room temperature ($|g_{MChD}|$ maxima: $0.0015\ T^{-1}$)[7] has hindered the development of solution-phase applications, such as enantioselective photochemical reactions and magnetically responsive chemical sensors.

To advance MChD-based engineering and science in the solution phase, we herein focused on designing systems that undergo transitions where the electric and magnetic dipole moments possess similar magnitudes and orientations.[7,25,29] Based on this strategy, chiral tetrakis-camphor-type Eu(III) complexes were prepared. These complexes contain four chiral trifluoroacetylcamphorate (tfc) ligands and one tetraethylammonium (TEA) cation (denoted as **(+)-Eu** and **(−)-Eu**; Fig. 1). These complexes exhibit a Laporte-forbidden emissive transition between their 4f orbitals, which gives rise to circularly polarized luminescence (CPL) with a remarkably high dissymmetry factor ($|g_{CPL}| \simeq 1.5$).[30] This high value is attributed to the similar magnitudes and orientations of the electric and magnetic transition dipole moments. The $|g_{MChD}|$ values of the Eu(III) complexes were estimated to be $0.015\ T^{-1}$, which is the

[a] Graduate School of Chemical Sciences and Engineering, Hokkaido University, Kita 13, Nishi 8, Kita-ku, Sapporo, Hokkaido, Japan
[b] Faculty of Engineering, Hokkaido University, Kita 13, Nishi 8, Kita-ku, Sapporo, Hokkaido, Japan. E-mail: y-kitagawa@eng.hokudai.ac.jp
[c] Institute for Chemical Reaction Design and Discovery (WPI-ICReDD), Hokkaido University, Kita 21, Nishi 10, Kita-ku, Sapporo, Hokkaido 001-0021, Japan
[d] Institute of Industrial Science, The University of Tokyo, 4-6-1 Komaba, Meguro-ku, Tokyo 153-8505, Japan
[e] Institute for Materials Research, Tohoku University, Katahira 2-1-1, Sendai 980-8577, Japan

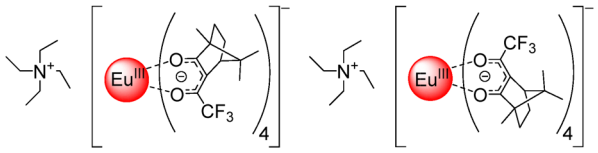

Fig. 1 Chemical structures of (left) **(+)-Eu** and (right) **(−)-Eu**.

highest among all reported maximum g_{MChD} values in the solution phase. Two additional tetrakis-type derivatives (Fig. S4), which also demonstrated large g_{MChD} values, confirmed the validity of the design strategy. This study provides new insights into the development of magneto-chiral photochemistry in solution at room temperature.

$TEA^+[Eu(+tfc)_4]^-$ (**(+)-Eu**) and $TEA^+[Eu(-tfc)_4]^-$ (**(−)-Eu**) were synthesized following a previously reported procedure,[30] and their purities were confirmed by elemental analysis (The synthesis and characterization methods are detailed in the SI). Single crystals of the **(+)-Eu** and **(−)-Eu** complexes were obtained by recrystallization from acetonitrile solution. The single crystal structures of **(+)-Eu**[30] and **(−)-Eu** are shown in Fig. 2, and the data are listed in Table 1. Based on the analyses of these crystal structures, the configuration of the camphorate ligands in **(+)-Eu** and **(−)-Eu** were categorized as the Λ and Δ forms, respectively.

To confirm the chiral structure in toluene solution, UV-vis and circular dichroism (CD) spectra of the **(+)-Eu** and **(−)-Eu** complexes were recorded. The broad absorption bands in the UV-vis spectra at approximately 310 nm are ascribed to the π–π* transition in the tfc aggregates around the Eu(III) ions (Fig. 3a). The CD spectra of **(+)-Eu** and **(−)-Eu** in toluene shows positive/negative and negative/positive CD signals from the longer-wavelength side at 310 nm, which are ascribed to exciton coupling between the tfc ligands (Fig. 3b). Time-dependent

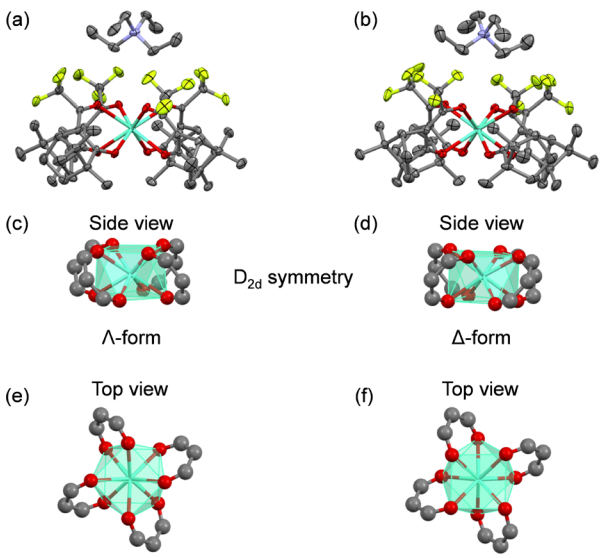

Fig. 2 ORTEP drawings of the tetrakis-type chiral Eu(III) complexes: (a, c, e) **(+)-Eu** and (b, d, f) **(−)-Eu**. The ellipsoid probability was set at 50%. Hydrogen atoms are omitted for clarity.

Table 1 Crystal data for **(+)-Eu** and **(−)-Eu**

	(+)-Eu	**(−)-Eu**
Formula	$C_{56}H_{76}EuF_{12}NO_8 + CH_3CN$	$C_{56}H_{76}EuF_{12}NO_8 + 2CH_3CN$
Crystal system	Orthorhombic	Orthorhombic
Space group	$P2_12_12_1$	$P2_12_12_1$
a/Å	14.2(2)	14.15(2)
b/Å	20.7(3)	20.97(3)
c/Å	20.9(3)	21.6(3)
α/deg.	90	90
β/deg.	90	90
γ/deg.	90	90
Volume/Å^3	6202.30(15)	6427.92(16)
Z	4	4
Density/g cm^{-1}	1.405	1.398
Temperature/K	123	123
R	0.0249	0.0278
wR^2	0.0710	0.0709

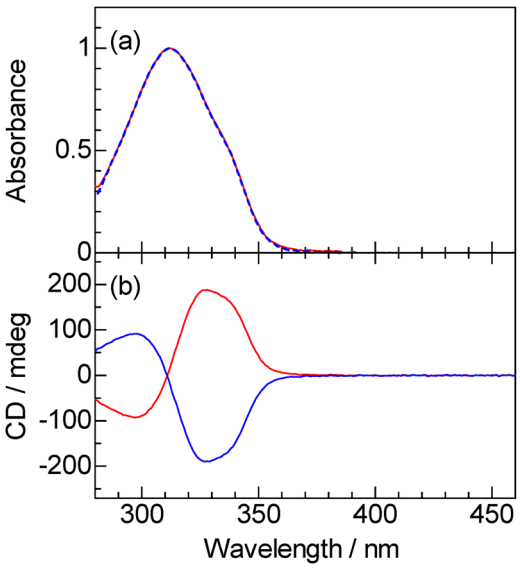

Fig. 3 UV-vis (a) and CD (b) spectra of the tetrakis-type chiral Eu(III) complexes (**(+)-Eu**: red curve, **(−)-Eu** (blue curve)) normalized by absorption maxima.

density functional theory (TD-DFT) calculations revealed that, in solution, the structures have same chiral structure (Λ/Δ) as in the solid state (Fig. S2).

The emission and CPL spectra of **(+)-Eu** and **(−)-Eu** in toluene are shown in Fig. 4a and b, respectively. The emission spectra exhibit two emission bands at 584 and 594 nm, which are identical for both enantiomers. These two bands originate from transitions from the $^5D_0$ level to the crystal-field-split $^7F_1$ levels, assigned to the A1 → A2 and A1 → E transitions, respectively, in the D_{2d}-symmetric Eu(III) complex.[31] From the CPL analysis, the $|g_{CPL}|$ factors were estimated as ∼ 0.54 for the A1 → A2 transition and ∼ 1.5 for the A1 → E transition, which quantify the degree of circular polarization. These large values indicate that the electric and magnetic transition dipole moments of the transition have similar magnitudes and orientations. The large static magnetic dipole moment in the final state, which is directly linked to the magnitude of the MChD

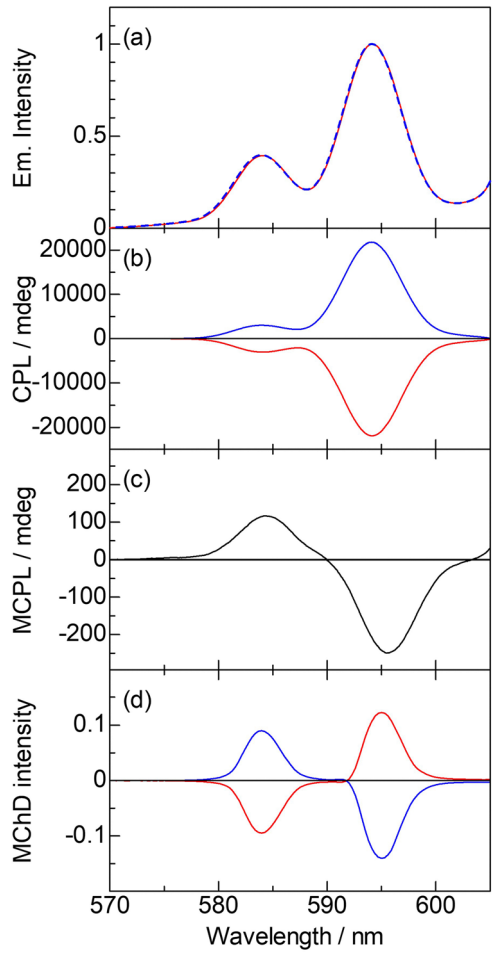

Fig. 4 (a) Emission, (b) CPL, (c) MCPL, and (d) MChD spectra for the tetrakis-type chiral Eu(III) complexes (**(+)-Eu**: red curve, **(−)-Eu**: blue curve, racemic state: black curve) normalized to the emission intensity maximum of the $^5D_0$ to $^7F_1$ transition band.

signal, was also confirmed by magnetic circularly polarized luminescence (MCPL) spectroscopy (Fig. 4c). Based on analyses of the MCPL spectra, the dissymmetric factors for the A1 → A2 and A1 → E transitions were estimated to be relatively large at ($|g_{MCPL}|$ ~ 1.2 × 10^{-2} T^{-1}) and ($|g_{MCPL}|$ ~ 1.3 × 10^{-2} T^{-1}), respectively.

The MChD spectra of **(+)-Eu** and **(−)-Eu** were acquired in toluene under an applied magnetic field of 15 T (Fig. 4d). These spectra revealed differences in luminescence intensity for the two emission bands centered at 584 and 594 nm, which were dependent on the direction of the magnetic field. The anisotropic factors ($|g_{MChD}|$ at 15 T) were calculated be 0.22 for the A1 → A2 transition (584 nm) and 0.19 for the A1 → E transition (597 nm). The g_{MChD} value for the A1 → A2 transition depends linearly on the magnetic field strength (Fig. 5, Fig. S3). The slope, calculated to be approximately ±0.015 T^{-1}, was more than ten times larger than the maximum value previously reported for solutions at room temperature.[7] To further validate our design, two structural analogs with large g_{CPL} values were synthesized (Fig. S4) and their MChD spectra were recorded in a solution system (Fig. S5). The strong MChD signals generated by the two compounds (up to $|g_{MChD}|$ = 0.016 T^{-1}) confirmed

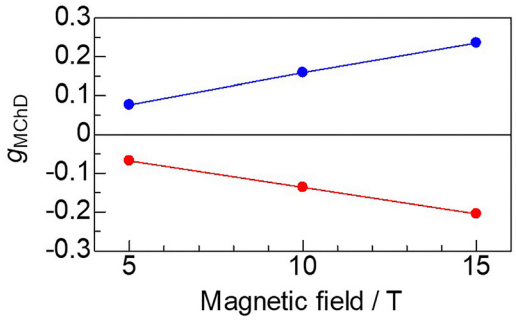

Fig. 5 Dependence of g_{MChD} on the magnitude of the magnetic field for the tetrakis-type chiral Eu(III) complexes (**(+)-Eu**: red line, **(−)-Eu**: blue line) evaluated for the A1 → A2 transition.

that the design based on the large g_{CPL} was effective. Furthermore, we evaluated the MChD spectrum for a room-temperature Eu(III) complex film with a different structural type (Fig. S8) that also exhibits large $|g_{CPL}|$ values (A1 → A2: 0.45, A1 → E: 1.2).[32] Notably, its $|g_{MChD}|$ values (A1 → A2: 1.2 × 10^{-2} T^{-1}, A1 → E: 9.6 × 10^{-3} T^{-1}) were found to follow the trend of the magnitude of its g_{CPL}, regardless of whether it was in the solution or film state (Fig. S9). Thus, we successfully developed an effective model for the development of solution-phase MChD applications.

To gain deeper insights, we focused on a detailed spectroscopic analysis of the MChD signals shown in Fig. 4d. The A1 → A2 transition at 584 nm in the MChD spectrum is consistent with those in the CPL and MCPL spectra (584 nm). The MChD signal associated with the A1 → A2 transition, which involves non-degenerate initial and final states, originates from the MChD B-term. In contrast, the A1 → E transition profiles in the MChD and MCPL spectra appear red-shifted to 596 nm relative to the corresponding CPL peak (594 nm). To elucidate the origin of this difference, the CPL, MCPL, and MChD spectra were subjected to Gaussian deconvolution (Fig. 6 and Fig. S6–S7). The fitting revealed that the CPL signal comprises two components[33] with the same sign (Fig. 6a), whereas the MCPL and MChD signals consist of two components with opposite signs (Fig. 6b and c). The dispersive MCPL signal corresponds to the Faraday A-term, which originates from the pseudo-degenerate final state (E).[1] In addition, the asymmetry in the positive/negative MCPL components is attributed to the Faraday B-term, arising from magnetic-field-induced mixing with the nearby A2 state. Similarly, the MChD signal for the A1 → E transition originates from the MChD A- and B-terms. The observed red-shifted MChD band (596 nm) results from the characteristic spectral overlay of these two terms, with a minor contribution from a slight Zeeman splitting of the E state under the applied magnetic field. Thus, we ascribed the larger $|g_{MChD}|$ of the A1 → A2 transition than that of the A1 → E transition to the strong absolute emission intensity and weakened $|g_{MChD}|$ in the A1 → E transition. Notably, tetrakis-type Eu(III) complexes coordinated with four β-diketonate ligands provided relatively strong crystal-field splitting. This results in a small energy gap (ΔE = 130 cm^{-1})

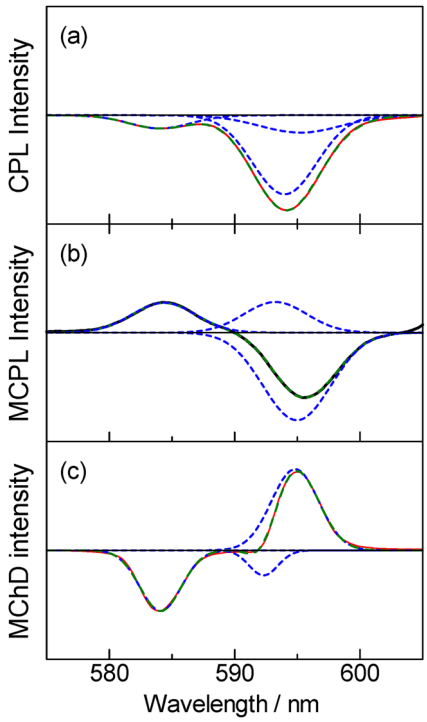

Fig. 6 Gaussian fitting results for the (a) CPL, (b) MCPL, and (c) MChD spectra of the tetrakis-type chiral Eu(III) complexes (**(+)-Eu**: red curve (a, c), racemic state: black curve (b)). Blue dashed lines represent individual fitting components, and the green dashed line represents the total fitting curve.

between the ground term ($^7F_0$) and the excited state ($^7F_1$(A2)). Such a small gap allows for significant thermal population in $^7F_1$(A2) at room temperature (293 K, >50%), making these complexes potential materials for demonstrating MChD-based asymmetric photochemical reactions induced by absorption *via* the transition from A2 to A1. Research into MChD-based asymmetric photochemical reactions using tetrakis-type Eu(III) complexes is currently underway.

We successfully demonstrated strong MChD signals in chiral tetrakis-type Eu(III) complexes in toluene at room temperature. The results confirmed that the present design strategy based on aligning the magnitudes and orientations of the electric and magnetic transition dipole moments is highly effective. The $|g_{MChD}|$ of 0.015 T^{-1} (0.22 at 15 T) for the 4f–4f transition of the Eu(III) center is the highest value reported to date for solution-phase systems. The validation of this model using structural analogs further confirmed that these systems are promising candidates for enhancing MChD effects. Thus far, various tetrakis-type Eu(III) complexes with four chiral β-diketonate ligands have been shown to exhibit large g_{CPL} values, facilitated by the optimized alignment of their transition dipole moments.[30,34–38] These results provide a crucial foundation for developing solution-phase applications such as asymmetric photochemical reactions and magnetically responsive chemical sensors operating under ambient conditions.

Y. Kitagawa supervised the project and designed the experiments. Syntheses and measurements were carried out by K. Itaya, K. Koizumi, and K. Inage. S. Kimura developed the MChD measurement system. All authors contributed to the discussion of the results and approved the final manuscript.

Conflicts of interest

There are no conflicts to declare.

Data availability

All of the other data supporting the findings of this study are available from the corresponding author upon reasonable request.

Supplementary information (SI) is available. See DOI: https://doi.org/10.1039/d6cc03254k.

CCDC 2550653 (**(−)-Eu**) and 2552135 (**(+)-Eu**) contain the supplementary crystallographic data for this paper.[39a,b]

Acknowledgements

This work was performed at HFLSM under the GIMRT Program of the Institute for Materials Research, Tohoku University (Proposal No. 202312-HMKPD-0044, 202411-HMKPD-0004, and 202512-HMKPD-0005). This work was supported by Grants-in-Aid for Scientific Research (grant numbers JP24K21774, JP23H04863, and JP20H02748). This work was also supported by the Adaptable and Seamless Technology Transfer Program through Target-driven R&D (A-STEP) from the Japan Science and Technology Agency (JST), Japan (Grant Number JPMJTR23T5), Iketani Science and Technology Foundation (Grant Number: 0371209-A), and the Institute for Chemical Reaction Design and Discovery (ICReDD), established by the World Premier International Research Center Initiative (WPI) of MEXT, Japan.

References

1 L. D. Barron, *Molecular Light Scattering and Optical Activity*. Cambridge University Press (2004).
2 B. P. Bloom, Y. Paltiel, R. Naaman and D. H. Waldeck, *Chem. Rev.*, 2024, **124**, 1950–1991.
3 A. Fert, N. Reyren and V. Cros, *Nat. Rev. Mater.*, 2017, **2**, 17031.
4 S.-W. Cheong and M. Mostovoy, *Nat. Mater.*, 2007, **6**, 13–20.
5 G. Wagnière and A. Meier, *Chem. Phys. Lett.*, 1982, **93**, 78–81.
6 L. D. Barron and J. Vrbancich, *Mol. Phys.*, 1984, **51**, 715–730.
7 G. L. J. A. Rikken and E. Raupach, *Nature*, 1997, **390**, 493–494.
8 G. L. J. A. Rikken and E. Raupach, *Phys. Rev. E: Stat. Phys., Plasmas, Fluids, Relat. Interdiscip. Top.*, 1998, **58**, 5081–5084.
9 G. L. J. A. Rikken and E. Raupach, *Nature*, 2000, **405**, 932–935.
10 M. S. Raju, M. Aragon-Albert, K. Cardenas, I. Breslavetz, G. L. J. A. Rikken, C. Train and M. Atzori, *ACS Cent. Sci.*, 2025, **11**, 1147–1153.
11 M. Saito, K. Ishikawa, K. Taniguchi and T. Arima, *Phys. Rev. Lett.*, 2008, **101**, 117402.
12 M. Atzori, I. Breslavetz, K. Paillot, K. Inoue, G. L. J. A. Rikken and C. Train, *J. Am. Chem. Soc.*, 2019, **141**, 20022–20025.
13 N. Nakagawa, N. Abe, S. Toyoda, S. Kimura, J. Zaccaro, I. G.-Luneau, D. Luneau, Y. Kousaka and A. Sera, *Phys. Rev. B*, 2017, **96**, 121102.
14 C. Train, R. Gheorghe, V. Krstic, L.-M. Chamoreau, N. S. Ovanesyan, G. L. J. A. Rikken, M. Gruselle and M. Verdaguer, *Nat. Mater.*, 2008, **7**, 729–734.
15 Y. Kitagawa, T. Miyatake and K. Ishii, *Chem. Commun.*, 2012, **48**, 5091–5093.

16 R. Sessoli, M.-E. Boulon, A. Caneschi, M. Mannini, L. Poggini, F. Wilhelm and A. Rogalev, *Nat. Phys.*, 2015, **11**, 69–74.
17 M. Atzori, F. Santanni, I. Breslavetz, K. Paillot, A. Caneschi, G. L. J. A. Rikken, R. Sessoli and C. Train, *J. Am. Chem. Soc.*, 2020, **142**(32), 13908–13916.
18 M. Atzori, K. Dhbaibi, H. Douib, M. Grasser, V. Dorcet, I. Breslavetz, K. Paillot, O. Cador, G. L. J. A. Rikken, B. L. Guennic, J. Crassous, F. Pointillart and C. Train, *J. Am. Chem. Soc.*, 2021, **143**, 2671–2675.
19 M. Atzori, H. D. Ludowieg, Á. V.-Pérez, M. Cortijo, I. Breslavetz, K. Paillot, P. Rosa, C. Train, J. Autschbach, E. A. Hillard and G. L. J. A. Rikken, *Sci. Adv.*, 2021, **7**, eabg2859.
20 X. Wang, S.-Q. Wang, J.-N. Chen, J.-H. Jia, C. Wang, K. Paillot, I. Breslavetz, L.-S. Long, L. Zheng, G. L. J. A. Rikken, C. Train, X.-J. Kong and M. Atzori, *J. Am. Chem. Soc.*, 2022, **144**, 8837–8847.
21 K. Dhbaibi, M. Grasser, H. Douib, V. Dorcet, O. Cador, N. Vanthuyne, F. Riobé, O. Maury, S. Guy, A. B. Ledoux, B. Baguenard, G. L. J. A. Rikken, C. Train, B. L. Guennic, M. Atzori, F. Pointillart and J. Crassous, *Angew. Chem., Int. Ed.*, 2023, **62**, e202215558.
22 M. S. Raju, K. Dhbaibi, M. Grasser, V. Dorcet, I. Breslavetz, K. Paillot, N. Vanthuyne, O. Cador, G. L. J. A. Rikken, B. L. Guennic, J. Crassous, F. Pointillart, C. Train and M. Atzori, *Inorg. Chem.*, 2023, **62**, 17583–17587.
23 C. Y. Li, L. C. Adi, K. Paillot, I. Breslavetz, L.-S. Long, L.-S. Zheng, G. L. J. A. Rikken, C. Train, X.-J. Kong and M. Atzori, *J. Am. Chem. Soc.*, 2024, **146**, 16389–16393.
24 M. S. Raju, K. Paillot, I. Breslavetz, G. Novitchi, G. L. J. A. Rikken, C. Train and M. Atzori, *J. Am. Chem. Soc.*, 2024, **146**, 23616.
25 L. C. Adi, O. G. Willis, A. Gabbani, G. L. J. A. Rikken, L. D. Bari, C. Train, F. Pineider, F. Zinna and M. Atzori, *Angew. Chem., Int. Ed.*, 2024, **63**, e202412521.
26 H. Lu, F. Qi, H. Wang, T. He, B. Sun, X. Gao, A. H. Comstock, S. Gull, Y. Zhang, T. Qiao, T. Shao, Y.-X. Zheng, D. Sun, Y. Chen, H.-L. Zhang, Z. Tang and G. Long, *Angew. Chem., Int. Ed.*, 2024, **64**, e202415363.
27 P.-X. Lu, L. C. Adi, P.-Y. Liao, W. Deng, H.-L. Wang, J.-H. Jia, G. L. J. A. Rikken, C. Train, M. Atzori and M.-L. Tong, *Angew. Chem., Int. Ed.*, 2026, e2565905.
28 Y. Kitagawa, H. Segawa and K. Ishii, *Angew. Chem., Int. Ed.*, 2011, **50**, 9133–9136.
29 N. B. Baranova and B. Y. Zeldovich, *Mol. Phys.*, 1979, **38**, 1085–1098.
30 M. Tsurui, R. Takizawa, Y. Kitagawa, M. Wang, M. Kobayashi, T. Taketsugu and Y. Hasegawa, *Angew. Chem., Int. Ed.*, 2024, **63**, e202405584.
31 J. H. Forsberg, *Coord. Chem. Rev.*, 1973, **10**, 195–226.
32 Y. Kitagawa, S. Wada, M. D. J. Islam, K. Saita, M. Gon, K. Fushimi, K. Tanaka, S. Maeda and Y. Hasegawa, *Commun. Chem.*, 2020, **3**, 119.
33 The two fitted CPL bands for the A → E transition indicate a slight splitting of the E state, which is caused by the formation of a weakly distorted square-antiprismatic structure.
34 J. L. Lunkley, D. Shirotani, K. Yamanari, S. Kaizaki and G. Muller, *J. Am. Chem. Soc.*, 2008, **130**, 13814–13815.
35 S. Di Pietro and L. Di Bari, *Inorg. Chem.*, 2012, **51**, 12007–12014.
36 J. L. Lunkley, D. Shirotani, K. Yamanari, S. Kaizaki and G. Muller, *Inorg. Chem.*, 2011, **50**, 12724–12732.
37 X. Zhang, X. Wang, W. Huang, S. Yin, T. Gao, Y. Zhou and H. Li, *Sci. Rep.*, 2025, **15**, 21738.
38 W. Huang, Z. Yao, S. Yin, T. Gao, J. Crassous, Y. Zhou and H. Li, *J. Am. Soc. Chem.*, 2026, **148**, 16931–16943.
39 (*a*) CCDC 2550653: Experimental Crystal Structure Determination, 2026, DOI: 10.5517/ccdc.csd.cc2rm54q; (*b*) CCDC 2552135: Experimental Crystal Structure Determination, 2026, DOI: 10.5517/ccdc.csd.cc2rnpy2.